Journal of Medical Systems (2018) 42: 7
https://doi.org/10.1007/s10916-017-0863-8

IMAGE & SIGNAL PROCESSING

# Correlation Filters for Detection of Cellular Nuclei in Histopathology Images

Asif Ahmad[1] · Amina Asif[1] · Nasir Rajpoot[2] · Muhammad Arif[3] · Fayyaz ul Amir Afsar Minhas[1]

Received: 15 November 2016 / Accepted: 13 November 2017 / Published online: 21 November 2017
© Springer Science+Business Media, LLC, part of Springer Nature 2017

**Abstract** Nuclei detection in histology images is an essential part of computer aided diagnosis of cancers and tumors. It is a challenging task due to diverse and complicated structures of cells. In this work, we present an automated technique for detection of cellular nuclei in hematoxylin and eosin stained histopathology images. Our proposed approach is based on kernelized correlation filters. Correlation filters have been widely used in object detection and tracking applications but their strength has not been explored in the medical imaging domain up till now. Our experimental results show that the proposed scheme gives state of the art accuracy and can learn complex nuclear morphologies. Like deep learning approaches, the proposed filters do not require engineering of image features as they can operate directly on histopathology images without significant preprocessing. However, unlike deep learning methods, the large-margin correlation filters developed in this work are interpretable, computationally efficient and do not require specialized or expensive computing hardware. *Availability*: A cloud based webserver of the proposed method and its python implementation can be accessed at the following URL: http://faculty.pieas.edu.pk/fayyaz/software.html#corehist.

**Keywords** Correlation filters · Kernelized correlation filters · Histopathology images · Cell detection · Nuclei detection

## Introduction

Nuclei detection in histopathology images is vital for assessment of tumors and cancers. Analysis of various properties of nuclei is an effective way to understand different stages of tumor progression [1–3]. Computerized methods have been rapidly evolving in the area of digital pathology to replace manual annotation for diagnostic assessment of histopathology images [4]. An automated system can identify and classify various types of cells in pathology images. Such systems offer substantial advantages over manual annotation in terms of accuracy, repeatability, time, and cost. However, detection of cells in stained histopathology images is a challenging task (see Fig. 1). For instance, complex tissue structures, nuclear pleomorphism (heterogeneous chromatin distribution and irregular boundaries), and variability in nuclei shape, size, and texture during nuclei life cycle complicate nuclei detection. Differences in slides preparation and image acquisition techniques along with variability in the staining process also pose difficulties in accurate automated detection of cells in histology images [4, 5].

Automated detection of cells in digital pathology images has gained immense interest from the research community over the last few decades. Existing work in the field can be broadly classified into two categories: *image processing based techniques* and *machine learning based methods*. Most of the work in literature has focused on image processing based segmentation techniques [6, 7]. Wang et al. proposed a semi-automatic segmentation method for detection of thyroid nuclei in feulgen stained histopathology images [7]. Their method

This article is part of the Topical Collection on *Image & Signal Processing*

✉ Asif Ahmad
asif.eng007@gmail.com

Amina Asif
a.asif.shah01@gmail.com

Nasir Rajpoot
n.m.rajpoot@warwick.ac.uk

Muhammad Arif
arif.gilgiti@pieas.edu.pk

Fayyaz ul Amir Afsar Minhas
afsar@pieas.edu.pk

[1] Biomedical Informatics Research Laboratory, Department of Computer and Information Sciences, Pakistan Institute of Engineering and Applied Sciences, PO Nilore, Islamabad, Pakistan

[2] Department of Computer Science, University of Warwick, Coventry, UK

[3] Department of Electrical Engineering, Pakistan Institute of Engineering and Applied Sciences, PO Nilore, Islamabad, Pakistan

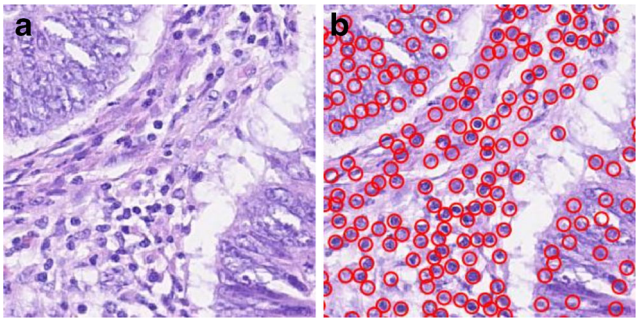


**Fig. 1** Visualization of cells in histopathology image (**a**) H&E stained Histopathology Image. **b** Encircled Nuclei in Histopathology image to be detected. Notice the large variation in morphologies across different nuclei

comprises three major steps: searching of closed rough contours using a graph cut method, refinement of contours to get segments and finally manual removal of incorrect segments by a pathologist. Chomphuwiset et al. employed the Hough-transform for detection of nuclei in H&E stained liver histology images [8]. However, their technique assumes spherical shaped nuclei and thus elongated shaped lymphocytes are not detected correctly. Yuan et al. proposed intensity thresholding followed by morphological operations, distance transform and watershed segmentation for nuclei detection [9]. However, this method is not suitable for segmenting nuclei in data containing large number of overlaps [3]. The technique by Jain et al. implements a region-based segmentation method followed by boundary-based cell detection technique to cope with the problem of irregular-shaped nuclei [10]. Their region-based segmentation involves thresholding and the use of watershed algorithm whereas boundary-based cell detection is done using an active contour model (ACM). Kumar et al. proposed a k-means segmentation algorithm for detection of cells in biopsy images of various tissues [6]. This method, however, is good only at detecting spherical shaped nuclei and does not work well for more complex morphologies.

A number of machine learning techniques have also been developed for detection of nuclei in histology images [3, 11–15]. Recent approaches in this domain have focused on deep learning algorithms. These methods typically rely on a deep architecture of multi-layered neural network to automatically learn features from large number of training examples [16]. Ciresan et al. deployed a deep neural network (DNN) as a pixel classifier to differentiate between mitotic and non-mitotic nuclei in breast cancer histopathology images [11]. Xie et al. proposed structural regression convolution neural network (CNN) for cells detection wherein strong response regions in the resulting proximity map indicate centroids of nuclei [17]. Xu et al. proposed a stacked sparse autoencoder strategy to learn high level features from patches of breast histopathology images and then classify these patches as nuclear or non-nuclear [18]. Recently, Sirinukunwattana et al. introduced locality sensitive deep learning approach for nuclei detection in H&E stained colorectal adenocarcinoma histology images. In this approach, a spatially constrained CNN is first employed to generate a probability map for a given input image using a sliding window strategy. Peak detection is then used for detection of nuclei in image patches [3].

Both machine learning and image processing or segmentation methods come with their own set of limitations. Segmentation techniques do not perform well in cases involving overlapping and clustered nuclei. The literature shows that significant attempts have been made to overcome these issues [19–27]. However, these problems still persist when dealing with images containing large number overlapping cells [4]. Another major issue associated with these methods is that most of these methods model nuclei as round or circular objects. This limits their applicability in cases involving irregularly shaped or elongated cells. Furthermore, image processing techniques require significant empirical tuning and hand-crafting. Deep learning approaches, on the other hand, do not rely on hand-crafted features and can be readily deployed for detection in datasets of complex images containing overlaps and variable shaped nuclei. However, these methods require a large amount of training data [16]. Computation requirements of these approaches are also large and they require expensive computational systems for implementation. Due to their black box nature, it is nearly impossible to understand the reasoning behind a prediction from these methods.

In this paper, we propose a novel correlation filter based approach for automated nuclei detection in histopathology images. Our proposed correlation filter based approach for nuclei detection is not only fast and simple but also requires only a small number of training images. This is due to the dependence of correlation filters on a very small set of parameters in comparison to deep learning techniques [28–30]. Like deep learning approaches, these filters are flexible and can detect complex or arbitrarily shaped nuclei without requiring hand-crafted features. Furthermore, the template for a trained correlation filter can be easily visualized to see the type of patterns the filter has learned. Our results show that these filters offer state of the art prediction performance in comparison to other existing techniques.

The rest of the paper is organized as follows. Second section gives details of the implementation of the proposed scheme together with the theory behind correlation filters. Third section presents the results and discussion while conclusions are given in fourth section.

## Materials and methods

### Mathematical formulation of correlation filters

A Correlation filter behaves as a classifier which learns target patterns in annotated training images and then finds similar

patterns in any test image using correlation. These filters employ Fast Fourier Transform (FFT) for performing correlation operations in the frequency domain which greatly reduces the computational cost of object detection [28]. Correlation filters have been widely used in object detection and tracking [28–33]. However, their use in the medical imaging domain has been very limited.

The fundamental principle behind the design of correlation filters is that the location(s) of target object(s) in an input image corresponds to peaks in the output of correlation of the input image with a template of the target object. A correlation filter is, in essence, a template of the target object obtained by training over a set of training images. Examples of correlation filters include Unconstrained Minimum Average Correlation Energy (UMACE) [34], Average of Synthetic Exact Filters (ASEF) [29] and Minimum Output Sum of Squared Error (MOSSE) [28], etc. MOSSE, due to built-in regularization, outperforms other correlation filters especially with small training data sets. Henriques et al. have recently published their work on kernelized correlation filters (KCF) for high speed tracking [30]. KCF uses non-linear kernels which allows for accurate detection of more complicated objects in comparison to the linear MOSSE filter.

Different correlation filter techniques differ, primarily, in the way they utilize training data for constructing the filter [29]. However, all these algorithms require a set of training images and their corresponding target images. A target image corresponding to a training image shows the locations of the target objects in the training image as peaks. An example of an input image can be seen in Fig. 1 together with annotations of known nuclei locations. A correlation filter can be conceptually visualized as an image whose correlation output with an input image is as close to the corresponding target image as possible [28]. Given a correlation filter $\boldsymbol{H}$, the correlation response $\boldsymbol{R}$ for an image $\boldsymbol{F}$ in the Fourier domain can be written as follows [35]:

$$\boldsymbol{R} = \boldsymbol{H}^* \odot \boldsymbol{F}. \tag{1}$$

Here, capital letters denote the Fourier domain representation, $\mathcal{F}(\cdot)$, of their corresponding spatial domain images, $\odot$ represents element-wise multiplication and $^*$ indicates the complex conjugate. The filter $\boldsymbol{H}$ can be obtained from training such that the correlation response of the filter for a given training image $\boldsymbol{F}$ is as close to its target image $\boldsymbol{G}$ as possible. In this study, we employ Minimum Output Sum of Squared Error (MOSSE) [28] and radial basis function (RBF) kernelized correlation filter (KCF) [30] for cells detection in histopathology images.

### Minimum output sum of squared error (MOSSE) filter

The MOSSE filter was proposed by Bolme et al. for high-speed object tracking and pedestrian detection [28, 30]. It finds an optimal regularized correlation filter $\boldsymbol{H}$, that minimizes the sum of squared error between the actual and the desired correlation responses. Given $N$ training images $\boldsymbol{f_i}$, $i = 1 \ldots N$, and their corresponding target images $\boldsymbol{g_i}$, the learning problem of MOSSE takes the form:

$$\boldsymbol{H}^* = \underset{\boldsymbol{H}^*}{\operatorname{argmin}} \left[ \sum_{i=1}^{N} \left\| \boldsymbol{F_i} \odot \boldsymbol{H}^* - \boldsymbol{G_i} \right\|^2 + \frac{\lambda}{2} \|\boldsymbol{H}\|^2 \right], \tag{2}$$

where $\lambda > 0$ represents the regularization parameter and $\|\cdot\|$ indicates the norm of an argument matrix. As stated earlier, the filter is chosen such that it minimizes the error between the desired correlation response $\boldsymbol{G_i}$ and the actual correlation output $\boldsymbol{R_i} = \boldsymbol{F_i} \odot \boldsymbol{H}^*$ for all training images. The regularization of the filter involves reducing the norm of the filter and it ensures filter stability especially in cases in which the number of training examples is small. The regularization parameter $\lambda$ controls the trade-off between the empirical error and regularization terms. The above optimization problem can be solved analytically and the closed form expression for the filter can be written as follows with the use of element-wise division operator $\oslash$:

$$\boldsymbol{H}^* = \left( \sum_{i=1}^{N} \boldsymbol{G_i} \odot \boldsymbol{F_i}^* \right) \oslash \left( \sum_{i=1}^{N} \boldsymbol{F_i} \odot \boldsymbol{F_i}^* + \lambda \right). \tag{3}$$

### Kernelized correlation filter (KCF)

Henriques et al. recently presented a non-linear extension of the MOSSE correlation filter for object tracking in videos and showed, via empirical results, that the non-linear or kernelized version of MOSSE is more accurate in tracking objects with complex patterns or morphologies [30]. Their derivation of the KCF follows a signal processing approach. In this paper, we present a complementary but simpler derivation of the KCF from a machine learning standpoint based on the Representer theorem [36, 37] and the kernel trick [38, 39].

Based on Eqs. (1) and (3), the response $\boldsymbol{R}$ of the MOSSE filter in the Fourier domain for a given test image $\boldsymbol{F}$ can be written in matrix form as:

$$\boldsymbol{R} = \boldsymbol{H}^* \odot \boldsymbol{F} = \left( \sum_{i=1}^{N} \boldsymbol{G_i} \odot \boldsymbol{F_i}^* \right) \oslash \left( \sum_{i=1}^{N} \boldsymbol{F_i} \odot \boldsymbol{F_i}^* + \lambda \right) \odot \boldsymbol{F}, \tag{4}$$

$$\boldsymbol{R} = \left( \sum_{i=1}^{N} \boldsymbol{G_i} \odot \boldsymbol{F_i}^* \odot \boldsymbol{F} \right) \oslash \left( \sum_{i=1}^{N} \boldsymbol{F_i} \odot \boldsymbol{F_i}^* + \lambda \right). \tag{5}$$

In accordance with the kernel trick and the Mercer theorem [40], the correlation inner-products ($\boldsymbol{F_i}^* \odot \boldsymbol{F}$ and $\boldsymbol{F_i} \odot \boldsymbol{F_i}^*$)

in Eq. (5) can be replaced by kernel correlation functions as follows:

$$\begin{aligned} \boldsymbol{R} &= \left(\sum_{i=1}^{N} \boldsymbol{G_i} \odot \boldsymbol{K}^{\boldsymbol{F}\boldsymbol{F_i}}\right) \oslash \left(\sum_{i=1}^{N} \boldsymbol{F_i} \odot \boldsymbol{F_i}^* + \lambda\right) \\ &= \sum_{i=1}^{N} \boldsymbol{K}^{\boldsymbol{F}\boldsymbol{F_i}} \odot \left(\boldsymbol{G_i} \oslash \left(\sum_{i=1}^{N} \boldsymbol{K}^{\boldsymbol{F_i}\boldsymbol{F_i}} + \lambda\right)\right) \\ &= \sum_{i=1}^{N} \boldsymbol{K}^{\boldsymbol{F}\boldsymbol{F_i}} \odot \boldsymbol{\alpha_i}. \end{aligned} \tag{6}$$

Here, $\boldsymbol{K}^{\boldsymbol{F}\boldsymbol{F_i}} = \boldsymbol{F} \odot \boldsymbol{F_i}^*$ is the kernel correlation of the test image $\boldsymbol{F}$ and the $i^{th}$ training image $\boldsymbol{F_i}^*$ and $\boldsymbol{K}^{\boldsymbol{F_i}\boldsymbol{F_i}} = \boldsymbol{F_i} \odot \boldsymbol{F_i}^*$ is the kernel auto-correlation of $\boldsymbol{F_i}$. The multiplicative factor $\boldsymbol{\alpha_i} = \boldsymbol{G_i} \oslash \left(\sum_{i=1}^{N} \boldsymbol{K}^{\boldsymbol{F_i}\boldsymbol{F_i}} + \lambda\right)$ is a term which is solely dependent on training image $i$. Any valid kernel function can be used for $\boldsymbol{K}$ and the introduction of these kernel functions allows for extension of the linear filter to non-linear one in an implicit manner. With a linear kernel function, $\boldsymbol{K}^{\boldsymbol{F}\boldsymbol{F_i}} = \boldsymbol{F} \odot \boldsymbol{F_i}^*$, the kernelized correlation filter is the same as the linear MOSSE filter. Other possible kernels include the Radial Basis Function (RBF) kernel given below [30].

$$\boldsymbol{K}_{\boldsymbol{rbf}}^{\boldsymbol{F}\boldsymbol{F_i}} = \mathcal{F}\left(exp\left(-\frac{1}{\sigma^2}\left(\|\boldsymbol{f}\|^2 + \|\boldsymbol{f_i}\|^2 - 2\mathcal{F}^{-1}\left(\boldsymbol{F} \odot \boldsymbol{F_i}^*\right)\right)\right)\right) \tag{7}$$

In this kernel, the hyper-parameter $\sigma$ controls the spread of the RBF and can be tuned for optimal performance and the exp operation is performed in an element-wise manner. It is important to note that the kernels in the KCF are in the Fourier domain and that a kernel function returns a matrix showing the correlation of its input arguments in an implicit Hilbert space. It is also interesting to observe that the response of the KCF is a manifestation of the Representer theorem. Specifically, since the objective function of the MOSSE filter is a regularized empirical risk function, the output response of the filter can be written as a linear combination $\sum_{i=1}^{N} \boldsymbol{K}^{\boldsymbol{F}\boldsymbol{F_i}} \odot \boldsymbol{\alpha_i}$ of kernel correlations evaluated on training images. This theoretical link renders several useful properties to Kernelized correlation filters. It shows that the Kernelized Correlation Filters are, in essence, a large margin classifier that operates directly over images without the need of feature engineering. It is also important to note that the KCF also optimizes the same objective function as a MOSSE filter by minimizing the empirical error between the target and filter output for all training examples and performing effective regularization. It also extends the applicability of correlation filters to multispectral images in which each band can have its own kernel which can then be combined via various kernel operations [41]. It also allows for multi-domain fusion of medical images and implicit feature transformations. Evaluating the kernels in the frequency domain through the Fast Fourier Transform (FFT) reduces computational complexity significantly without any loss in accuracy [42]. Equations (3), (4) and (6) form the core of our proposed scheme.

## Proposed method

The details of individual steps in the proposed method is given below.

### Histopathology image dataset and construction of target images

The dataset used in this study consists of 100 hematoxylin & eosin (H&E) stained histopathology images of colorectal adenocarcinomas which has been organized, used and published online by Sirinukunwattana et al. [3]. All these images are 500 × 500 pixels in size and have been cropped from non-overlapping areas of 10 whole-slide images that were obtained from nine patients. Each image in the dataset is provided with annotations of nuclei locations as shown in Fig. 1 for a representative image. There are a total of 29, 756 nuclei in the dataset. Note that the dataset contains complex and wide variety shapes of nuclei where overlap is also present. We have used this data set as it allows us to compare our technique directly with the current state of the art techniques in the field which have already been benchmarked on this data set by Sirinukunwattana et al.

For construction of a correlation-filter, we need $N$ training images $\boldsymbol{f_i}$, $i = 1 \ldots N$, and their corresponding target images $\boldsymbol{g_i}$. We constructed a target image, $\boldsymbol{g_i}$, for each given image by placing a Gaussian of size $\sigma = 2$ at all annotated cell locations (see Fig. 2). This Gaussian blurring helps avoid ringing artifacts associated with frequency domain manipulation [43, 44].

### Pre-processing

An important step in design of correlation filters is the preprocessing of images. First, the hematoxylin channel is extracted from the images for further analysis using a Python package based on color deconvolution [45]. This is because the hematoxylin dye is basic in nature and binds to the acidic DNA or RNA in the nucleus during the staining process. Second, a log transformation is applied to reduce the effect of shadows and lightening variations. Third, pixel values are normalized to have a mean of 0.0 and norm of 1.0 to give images a consistent intensity [28, 29]. Edge-padding is then performed in which all images are padded with additional pixels on all sides. Finally, the image is multiplied by a Tukey window which reduces pixel values near the edges to zero while preserving all other pixels values in their original form [46]. Edge-padding followed by Tukey windowing helps cope with edge

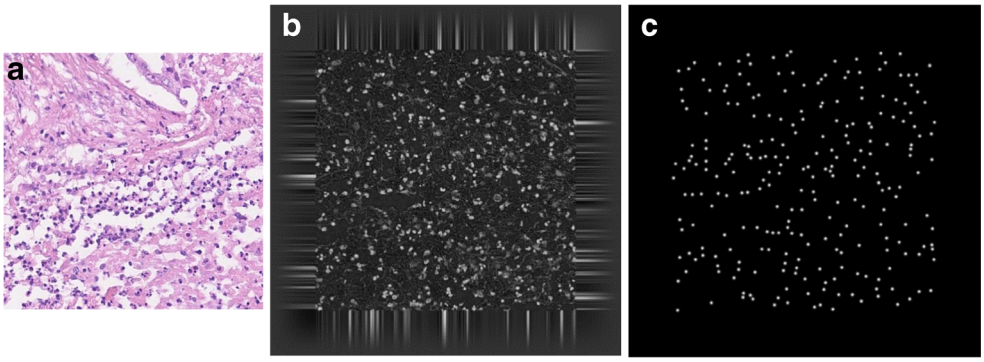


**Fig. 2** An illustration of preprocessing step. **a** Histopathology Image. **b** Preprocessed Hematoxylin (Featured) Image. **c** Preprocessed Desired Target Image

artifacts associated with FFT operations used in correlation filter design [28, 29]. These additional padded pixels are removed after the filter response has been calculated. Figure 2 shows the original training image along with its pre-processed version and the desired target image.

### Correlation filter construction and detection

After preprocessing of images and their corresponding targets, we designed MOSSE and RBF correlation filters based on Eqs. (3), (4) and (6). The filter response for an input image can be obtained by Eq. (6) and converted to the spatial domain by taking inverse FFT. Peaks in the spatial domain response image are interpreted as putative nuclei locations. The hyper-parameters $\lambda$ and $\sigma$ of the correlation filters are tuned based on statistical performance metrics over training images only.

### Performance evaluation and parameter tuning

Precision, Recall and F1 score are used as performance metrics in this work to assess the performance of correlation filter based detection and to carry out comparison with other detection approaches [47]. We followed the same two-fold cross-validation procedure for performance evaluation as done in [3]. Locations of peaks in the response image are compared to their known locations for images in the testing fold using a 6-pixel distance criterion and Precision, recall and F1-score are averaged over all test images to get averaged statistics which describe the quantitative performance of correlation filter based detection.

**Table 1** 2-fold cross validation results of detection approaches

| Detection approach | Precision | Recall | F1 score |
|---|---|---|---|
| **Baseline** | 0.45 | 0.74 | 0.55 |
| **RBF Correlation Filter** | **0.83** | **0.86** | **0.84** |
| **Linear MOSSE Filter** | **0.76** | **0.88** | **0.81** |
| SC-CNN (M = 1) [3] | 0.76 | 0.83 | 0.79 |
| SC-CNN (M = 2) [3] | 0.78 | 0.82 | 0.80 |
| CP-CNN [3] | 0.70 | 0.69 | 0.69 |
| SR-CNN [22] | 0.78 | 0.80 | 0.79 |
| SSAE [18] | 0.62 | 0.64 | 0.63 |
| LIPSyM [48] | 0.72 | 0.52 | 0.60 |
| CRImage [9] | 0.66 | 0.46 | 0.54 |

The bold entries represent the highest values of precision, recall and F1 score.

## Results and discussion

Table 1 shows the results for two-fold cross validation results of correlation filter based detection along with other recently published detection algorithms [3]. Note that the evaluation protocol of our approach is the same as other comparative methods which leads to a fair comparison.

As a baseline, we considered an optimal-threshold based binarization of the Hemotoxylin image which gives an F1 score of 0.55. Since the Hemotoxylin dye binds DNA, therefore the Hemotoxylin component of the input image shows a high-valued response at locations corresponding to nuclei. The baseline corresponds to the results obtained if no filter learning is performed and the Hemotoxylin component of the input image is directly used for detection of nuclei. Our results show that both linear (MOSSE) and RBF correlation (KCF) filters give significantly improvement in prediction performance over the baseline.

It is also evident form Table 1 that correlation filter based approaches outperform all other recently published approaches for detection of nuclei in the given histopathology images. Here, we see that F1 score of our proposed filters has

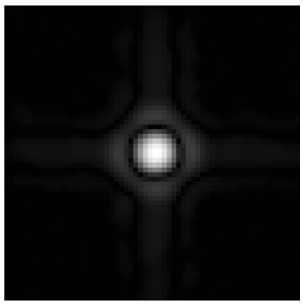

**Fig. 3** Visualization of MOSSE Filter in spatial domain

surpassed deep learning and segmentation approaches. In comparison to the state of the art approaches such as SC-CNN and SR-CNN, our KCF based approach offers a substantial improvement in prediction accuracy. Our proposed algorithm does not require feature or process engineering needed by image processing based techniques or regular machine learning methods as it operates directly on the Hemotoxylin image. RBF KCF offers the highest sensitivity and precision scores which clearly shows that it can detect nuclei with complex morphologies better than all other techniques. The proposed scheme is significantly better than deep learning techniques in terms of resource requirements and computational complexity as well. It does not require expensive hardware for training or testing. Cross-validation over a standard Core i3 system with 6GB RAM requires only 18 s for the linear and 54 s for the RBF KCF. Furthermore, in contrast

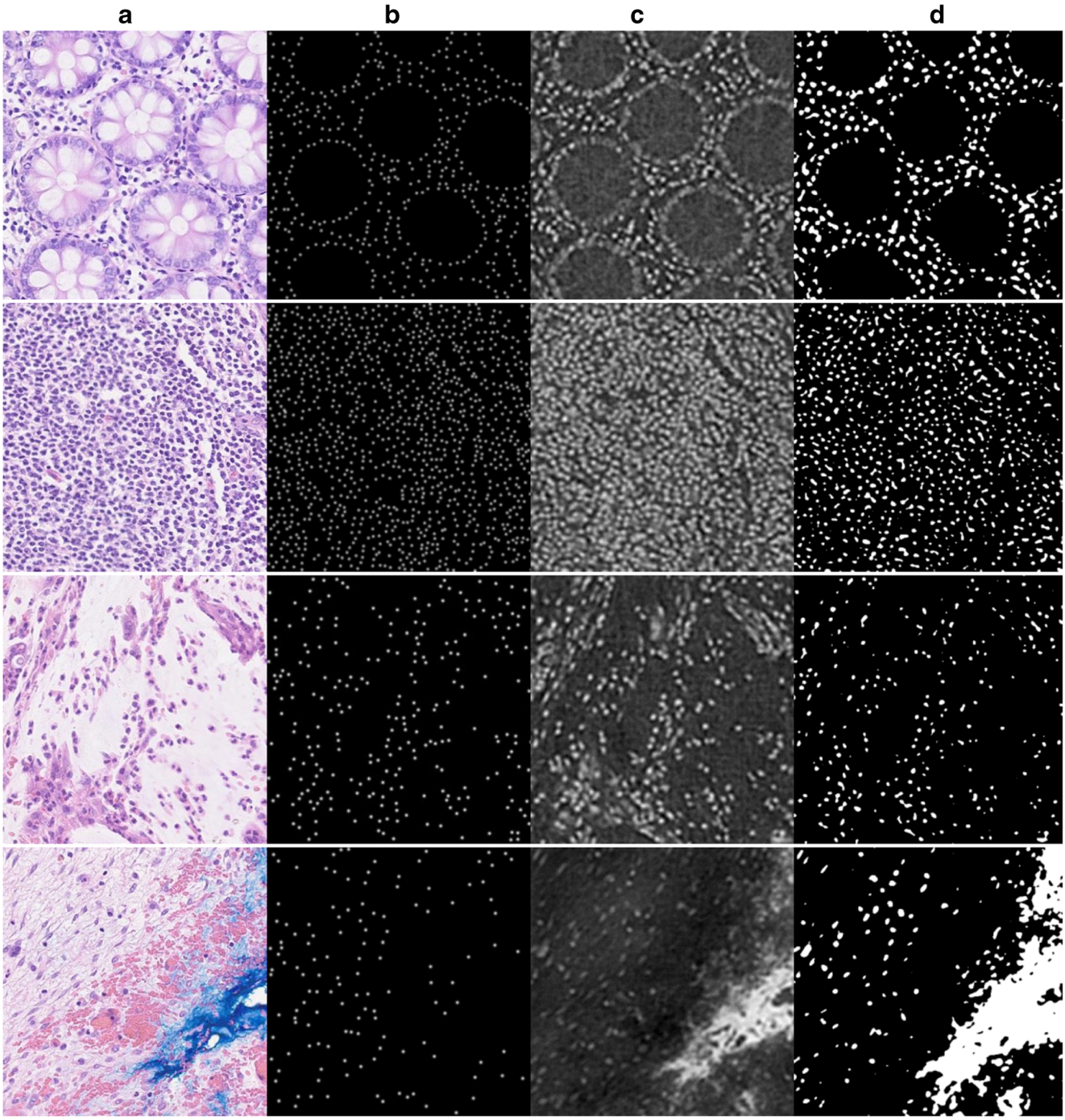


**Fig. 4** **a** Test Images. **b** Desired Target Images (Ground Truth Regions). **c** Correlation Response Images obtained with RBF Filter (**d**) Binarized RBF Response images showing peak locations only

to existing deep learning methods, the proposed scheme operates over complete images and not over patches. This eliminates the need for window-based processing.

The template learned by the MOSSE filter can be visualized as well which gives us some insight into the working of the algorithm. The trained filter zoomed-in to capture essential details of the template is shown in Fig. 3. Its symmetric shape with a central round region surrounded by a band resembles an ideal cell with the nucleus in the middle. However, it does not fully conform to any specific cellular morphology and appears to be a combination of different morphologies. This figure also illustrates the interpretability and intuitive nature of the proposed filter.

A qualitative analysis of the proposed approach is shown in Fig. 4. It shows various input images together with their target and output images. It can be clearly seen that the proposed scheme can detect nuclei in input images of varying nuclei densities and morphologies. The top 3 rows show images on which the precision and recall of the KCF is high whereas the bottom row shows an image in which the KCF, along with other detection methods used in comparison, fail to detect cells in the region which has issues due to the staining process. This highlights the limitation of all nuclei detection approaches.

We also experimented with changing the amount of training data for the Kernelized correlation filter. This was done by changing the cross-validation strategy from 2-fold to leave-one-image-out in which the filter is trained on all available images except for one which is held out for training. This process is repeated for all training images and the performance statistics for individual images are then averaged. We noticed only a small improvement in prediction accuracy: the average F1 score improved from 0.84 to 0.86. This clearly shows that the proposed scheme is stable with respect to changes in data and that it does not need large amounts of training data to deliver optimal performance.

## Conclusions

In this study, we have presented a correlation filter based approach for automated detection of cells and nuclei in stained histopathology images of colorectal adenocarcinomas. The proposed method offers significant advantages over existing methods in terms of accuracy, speed, interpretability, and flexibility in handling different nuclear morphologies. It also opens the avenue for applying correlation filters to related problems in biomedical imaging. We have made the code of the Python implementation of our proposed method available for download. The proposed scheme is also available as a web-server in which the user can submit their H&E stained histology image and obtained the response image from our filter. Both these implementations are accessible via the URL: http://faculty.pieas.edu.pk/fayyaz/software.html#corehist

**Funding** Asif Ahmed is funded by a fellowship from the Pakistan Institute of Engineering and Applied Sciences. Amina Asif acknowledges the funding support from the IT and Telecom Endowment Fund at Pakistan Institute of Engineering and Applied Sciences.

**Compliance with Ethical Standards**

**Conflict of Interest** The authors declare no conflict of interest.

**Ethical Approval** This article does not contain any studies with human participants or animals performed by any of the authors.

## References

1. Demir, C., and Yener, B., Automated cancer diagnosis based on histopathological images: a systematic survey. In: *Dept Comput Sci Rensselaer Polytech. Inst. Troy NY USA Tech Rep TR-05-09*, 2005.
2. Dunne, B., and Going, J.J., Scoring nuclear pleomorphism in breast cancer. *Histopathology.* 39(3):259–265, Sep. 2001.
3. Sirinukunwattana, K., Raza, S.E.A., Tsang, Y.W., Snead, D.R.J., Cree, I.A., and Rajpoot, N.M., Locality sensitive deep learning for detection and classification of nuclei in routine colon cancer histology images. *IEEE Trans. Med. Imaging*. 35(5):1196–1206, 2016.
4. Irshad, H., Veillard, A., Roux, L., and Racoceanu, D., Methods for nuclei detection, segmentation, and classification in digital histopathology: A review-current status and future potential. *IEEE Rev. Biomed. Eng.* 7:97–114, 2014.
5. Vahadane, A., and Sethi, A., Towards generalized nuclear segmentation in histological images. In: *Bioinformatics and Bioengineering (BIBE), 2013 I.E. 13th International Conference on*, pp. 1–4, 2013.
6. Kumar, R., Srivastava, R., and Srivastava, S., Detection and classification of cancer from microscopic biopsy images using clinically significant and biologically interpretable features. *J. Med. Eng.* 2015:e457906, 2015.
7. Wang, W., Ozolek, J.A., and Rohde, G.K., Detection and classification of thyroid follicular lesions based on nuclear structure from histopathology images. *Cytometry A*. 9999A:NA-NA, 2010.
8. Chomphuwiset, P., Magee, D.R., Boyle, R.D., and Treanor, D., Context-based classification of cell nuclei and tissue regions in liver histopathology. In: *MIUA*, pp. 239–244, 2011.
9. Yuan, Y., et al., Quantitative image analysis of cellular heterogeneity in breast tumors complements genomic profiling. *Sci. Transl. Med.* 4(157):157ra143, 2012.
10. Jain, A., Atey, S., Vinayak, S., and Srivastava, V., Cancerous cell detection using histopathological image analysis. *Int. J. Innov. Res. Comput. Commun. Eng.* 2(12):7419–7426, 2015.
11. Cireşan, D.C., Giusti, A., Gambardella, L.M., and Schmidhuber, J., Mitosis detection in breast cancer histology images with deep neural networks. In: *International Conference on Medical Image Computing and Computer-assisted Intervention*, pp. 411–418, 2013.
12. Mao, K.Z., Zhao, P., and Tan, P.-H., Supervised learning-based cell image segmentation for p53 immunohistochemistry. *IEEE Trans. Biomed. Eng.* 53(6):1153–1163, 2006.
13. Sommer, C., Fiaschi, L., Hamprecht, F.A., and Gerlich, D.W., Learning-based mitotic cell detection in histopathological images. In: *Pattern Recognition (ICPR), 2012 21st International Conference on*, pp. 2306–2309, 2012.
14. Veillard, A., Kulikova, M.S., and Racoceanu, D., Cell nuclei extraction from breast cancer histopathologyimages using colour, texture, scale and shape information. *Diagn. Pathol.* 8(Suppl 1):S5, 2013.

15. Vink, J.p., Van Leeuwen, M.b., Van Deurzen, C.h.m., and De Haan, G., Efficient nucleus detector in histopathology images. *J. Microsc.* 249(2):124–135, 2013.
16. Madabhushi, A., and Lee, G., Image analysis and machine learning in digital pathology: Challenges and opportunities. *Med. Image Anal.* 33:170–175, 2016.
17. Xie, Y., Xing, F., Kong, X., Su, H., and Yang, L., Beyond classification: Structured regression for robust cell detection using convolutional neural network. In: Navab, N., Hornegger, J., Wells, W.M., and Frangi, A.F. (Eds.), *Medical Image Computing and Computer-Assisted Intervention – MICCAI 2015*. Springer International Publishing, pp. 358–365, 2015.
18. Xu, J., et al., Stacked sparse autoencoder (SSAE) for nuclei detection on breast cancer histopathology images. *IEEE Trans. Med. Imaging*. 35(1):119–130, 2016.
19. Ali, S., Veltri, R., Epstein, J.I., Christudass, C., and Madabhushi, A., Adaptive energy selective active contour with shape priors for nuclear segmentation and gleason grading of prostate cancer. In: *International Conference on Medical Image Computing and Computer-Assisted Intervention*, pp. 661–669, 2011.
20. Ali, S., and Madabhushi, A., An integrated region-, boundary-, shape-based active contour for multiple object overlap resolution in histological imagery. *IEEE Trans. Med. Imaging*. 31(7):1448–1460, Jul. 2012.
21. Al-Kofahi, Y., Lassoued, W., Lee, W., and Roysam, B., Improved automatic detection and segmentation of cell nuclei in histopathology images. *IEEE Trans. Biomed. Eng.* 57(4):841–852, Apr. 2010.
22. Jung, C., Kim, C., Chae, S.W., and Sukjoong, O., Unsupervised segmentation of overlapped nuclei using Bayesian classification. *IEEE Trans. Biomed. Eng.* 57(12):2825–2832, Dec. 2010.
23. Di Cataldo, S., Ficarra, E., Acquaviva, A., and Macii, E., Automated segmentation of tissue images for computerized IHC analysis. *Comput. Methods Programs Biomed.* 100(1):1–15, Oct. 2010.
24. Huang, P.-W., and Lai, Y.-H., Effective segmentation and classification for HCC biopsy images. *Pattern Recognit.* 43(4):1550–1563, Apr. 2010.
25. Kong, H., Gurcan, M., and Belkacem-Boussaid, K., Partitioning histopathological images: An integrated framework for supervised color-texture segmentation and cell splitting. *IEEE Trans. Med. Imaging*. 30(9):1661–1677, Sep. 2011.
26. Mouelhi, A., Sayadi, M., and Fnaiech, F., c. In: *Communications, Computing and Control Applications (CCCA), 2011 International Conference on*, pp. 1–6, 2011.
27. Wienert, S., et al., Detection and segmentation of cell nuclei in virtual microscopy images: A minimum-model approach. *Sci. Rep.* 2:503, 2012.
28. Bolme, D.S., Beveridge, J.R., Draper, B.A., and Lui, Y.M., Visual object tracking using adaptive correlation filters. In: *Computer Vision and Pattern Recognition (CVPR), 2010 I.E. Conference on*, pp. 2544–2550, 2010.
29. Bolme, D.S., Draper, B.A., and Beveridge, J.R., Average of synthetic exact filters. In: *Computer Vision and Pattern Recognition, 2009. CVPR 2009. IEEE Conference on*, pp. 2105–2112, 2009.
30. Henriques, J.F., Caseiro, R., Martins, P., and Batista, J., High-speed tracking with kernelized correlation filters. *Pattern Anal. Mach. Intell. IEEE Trans. On*. 37(3):583–596, 2015.
31. Boddeti, V. N., Kanade, T., and Kumar, B. V. K. V., Correlation Filters for Object Alignment. 2013, pp. 2291–2298.
32. Danelljan, M., Hager, G., Shahbaz Khan, F., and Felsberg, M., Learning spatially regularized correlation filters for visual tracking. In: *Proceedings of the IEEE International Conference on Computer Vision*, pp. 4310–4318, 2015.
33. Savvides, M., Kumar, B. V., and Khosla, P., Face verification using correlation filters. *3rd IEEE Autom. Identif. Adv. Technol.*, 56–61, 2002.
34. Savvides, M. and Kumar, B. V. K. V., Efficient design of advanced correlation filters for robust distortion-tolerant face recognition. In: *IEEE Conference on Advanced Video and Signal Based Surveillance, 2003. Proceedings,* 2003, pp. 45–52.
35. Proakis, J.G., and Manolakis, D.K., *Digital Signal Processing*, 4th edn. N.J: Pearson, Upper Saddle River, 2006.
36. Schölkopf, B., Herbrich, R., and Smola, A.J., A generalized representer theorem. In: Helmbold, D., and Williamson, B. (Eds.), *Computational Learning Theory.* Springer, Berlin Heidelberg, pp. 416–426, 2001.
37. Schölkopf, B. and Smola, A. J., *Learning with Kernels: Support Vector Machines, Regularization, Optimization, and Beyond*. MIT Press, 2002.
38. Hofmann, M., Support vector machines—Kernels and the kernel trick. *Notes*. 26, 2006.
39. Jäkel, F., Schölkopf, B., and Wichmann, F.A., A tutorial on kernel methods for categorization. *J. Math. Psychol.* 51(6):343–358, 2007.
40. Shawe-Taylor, J., and Cristianini, N., *Kernel Methods for Pattern Analysis*. Cambridge University Press, 2004.
41. Schölkopf, B., and Burges, C.J.C., *Advances in Kernel Methods: Support Vector Learning*. MIT Press, 1999.
42. Rao, K.R., Kim, D.N., and Hwang, J.-J., *Fast Fourier Transform - Algorithms and Applications*, 1st edn. Springer Publishing Company, Incorporated, 2010.
43. Bankman, I.N., *Handbook of Medical Imaging: Processing and Analysis Management*. Academic Press, 2000.
44. Chitode, J.S., *Digital Signal Processing*. Technical Publications, 2009.
45. Ruifrok, A.C., and Johnston, D.A., Quantification of histochemical staining by color deconvolution. *Anal. Quant. Cytol. Histol. Int. Acad. Cytol. Am. Soc. Cytol.* 23(4):291–299, 2001.
46. Harris, and Fredric, J., On the use of windows for harmonic analysis with the discrete Fourier transform. *Proc. IEEE*:51–83, 1978.
47. Alpaydin, E., *Introduction to Machine Learning*. MIT Press, 2014.
48. Kuse, M., Kalasannavar, V., Rajpoot, N., Wang, Y.-F., and Khan, M., Local isotropic phase symmetry measure for detection of beta cells and lymphocytes. *J. Pathol. Inform.* 2(2):2, 2011.